

An epidemic model highlighting humane social awareness and vector–host lifespan ratio variation*

Karunia Putra Wijaya¹, Joseph Páez Chávez^{2,1}, and Dipo Aldila^{3,*}

¹*Mathematical Institute, University of Koblenz, 56070 Koblenz, Germany*

²*Center for Applied Dynamical Systems and Computational Methods (CADSCOM), Faculty of Natural Sciences and Mathematics, Escuela Superior Politécnica del Litoral, P.O. Box 09-01-5863, Guayaquil, Ecuador*

³*Department of Mathematics, University of Indonesia, 16424 Depok, Indonesia*

*Corresponding author. Email: aldiladipo@sci.ui.ac.id

Many vector-borne disease epidemic models neglect the fact that in modern human civilization, social awareness as well as self-defence system are overwhelming against advanced propagation of the disease. News are becoming more effortlessly accessible through social media and mobile apps, while apparatuses for disease prevention are inclined to be more abundant and affordable. Here we study a simple host–vector model in which media-triggered social awareness and seasonality in vector breeding are taken into account. There appears a certain threshold indicating the alarming outbreak; the number of infective human individuals above which shall actuate the self-defence system for the susceptible subpopulation. A model where the infection rate revolves in the likelihood of poverty, reluctance, tiresomeness, perceiving the disease as being easily curable, absence of medical access, and overwhelming hungrier vectors is proposed. Further discoveries are made from undertaking disparate time scales between human and vector population dynamics. The resulting slow–fast system discloses notable dynamics in which solution trajectories confine to the slow manifold and critical manifold, before finally ending up at equilibria. How coinciding the slow manifold with the critical manifold enhances periodic forcing is also studied. The finding on hysteresis loops gives insights of how defining alarming outbreak critically perturbs the basic reproductive number, which later helps keep the incidence cycle on small magnitudes.

Keywords: vector-borne disease, media-triggered social awareness, slow–fast system, critical manifold, periodic system

1 Introduction

World population has witnessed social and monetary misfortunes from the spreading of vector-borne diseases since subsequent centuries [1, 2, 3]. Many intervention strategies have been researched and implemented to fight against the diseases, most of which are based on suppressing vector population and shielding humans from contacts with vectors [4, 5]. Despite learnable seasonality of the prominent meteorological factors, therefore of the vector population, the disease-related incidences continue to remain cyclical [6]. Questionable here are thus, the sureness and regularity in implementing such intervention strategies.

Media reports have played a significant role in influencing individuals' states of mind and practices during epidemics [7, 8], keeping them aware of surrounding infection threats. Such computerized information nowadays is openly accessible from numerous sources including direct news from broad communications (e.g. radios, televisions, newspapers, booklets) and catchphrases/hashtags from social media (e.g. Facebook, Twitter, Instagram). The latter can especially gauge further detailed information including geospatial labels into a certain sphere only under short typing. The main task of the media in the context of anti-disease campaign is to scatter incidence data and regularly flag up related themes including possible causes, symptoms, worsening effects, data forecasts, clinical accessibility, prevention strategies, and emergent solutions [9, 10]. It is a moderately modest method for reporting

centralized information regarding neighbours' wellbeing and can certainly return much broader influence, notwithstanding that outbreak data can be hardly accessible through personal approaches. In response, individuals educated by media can play safe ranging from injecting vaccines, smearing repellent fluids, wearing defensive clothing, to staying away from social contacts with infected humans and from endemic regions [10]. Educated infective humans may likewise take measures to ban themselves from being exposed to others to diminish infectivity.

Recently, a number of modeling studies have been done to evaluate the impacts of media reports on the change of individual conducts against the spread of infectious diseases. Except the statistical distribution-matching [11], classical linear regression [12] and game-theoretic approach [13], the existing mathematical models in this context engineer differential equations – typically SIR-type models – as to govern incidence pattern. The latter mostly fall into two ideas. The first idea highlights media as to give feedback to a system for the infectivity lessens as the number of infective individuals gets larger. Placement of the corresponding measures depends on the types of actions taken against the disease spread. In case of vaccination-like preventive actions, the feedback serves as a rate in taking up susceptible hosts [14]. In case of repellence against contacts, it usually serves as modification of the infection or contact rate. To this later case, the infection rate is likely to be a decreasing function of the infective (and exposed) subpopulation, which can be either a rational function [15, 16, 17], an exponential function [18, 19, 8] or a rather generalized version [20]. The second idea includes the introduction of “aware” subpopulation from the original susceptible, infected, and recovered subpopulation [21, 22, 23]. The rate at which an “unaware” individual becomes “aware” can thus be modeled as an (increasing) function of the infective host subpopulation [14] and/or a certain measure for the intensiveness of media reports [24, 23, 25, 21]. Another view also sees a two-way relationship, as such intensiveness increases along with an increasing number of incidences [24, 21].

In this paper, we present a model that follows the first idea. The governing equations are, possibly the simplest SISUV model with constant host population and saturating vector population. A novelty here is the introduction of an alarming incidence level j^* , below which medical departments can never transfer information to media holders for either time, interest, or financial restrictions. We further develop two models for the infection rate. The first model portrays a non-increasing infection rate, which is based on the situation where the hosts keep up the pace in taking up preventive measures along with ever-streaming media reports. Notwithstanding different treatment in the model, previous investigation [15] equivalently indicates the supercritical-type of bifurcation of the model system. The second model considers the scenario where the alarming outbreak j^* is defined as the maximum number of patients the available hospitals in the observed region can accommodate. The case that the disease is endemic in “developing” regions also sets additional factors why human's exposure to infection can get higher with the incidence level. The infection rate accordingly decreases due to media reports, yet it revolves as the incidence level gets higher due to poverty, reluctance in taking up preventive measures, tiresomeness, perceiving the disease as being easily curable, absence of medical access, and presence of hungrier vectors.

For more realistic touching, we include a seasonal forcing in the vector population due to meteorological factors. Periodical climatic patterns have been argued to be one of the most influential conditions that catalyze the infection processes [26, 27]. This stems from the observation that disease vectors essentially look for the most favorable ambient temperature, humidity, wind speed and water precipitation surrounding their life cycle [28, 29]. In some tropical and subtropical regions, for example Jakarta, Indonesia [6], Taiwan [30] and Sisaket, Thailand [31], meteorological factors might be too random under a small time scale, but they often exhibit apparent long-term trends with certain periodicities. At this point, the behavior of meteorological factors, and therefore that of incidence levels, become more “understandable”. This fact gives us useful information for more accurate forecasts and the implementation of disease controls.

However, due to a natural discrepancy on the lifespans of vector and host, such model might portray significantly different solution trajectories under the variation of the lifespan ratio ϵ . Added with another assumption on the infection rates, the ratio variation gives birth to a singularly perturbed system. This allows the field of the vector dynamics to entirely be controlled by ϵ . Two traditional results are underlying: critical manifold, the surface representing the equilibrium of the system under

the assumption that the vector lifespan is infinitesimal ($\epsilon = 0$), and slow manifold, a (locally attractive) surface as perturbation of the critical manifold in case of full stability for $\epsilon > 0$. Therefore, as the reminder we go towards answering the following questions: What is the stability status of the critical manifold? How can solution trajectories confine to the slow manifold, before approaching the critical manifold and ultimately a stable equilibrium? How is the slow manifold approximated? How many are and how are the stability statuses of the endemic equilibria? How do the periodic solutions behave with respect to the basic reproductive number and the alarming incidence level? How to see if the periodic solutions expand with the amplitude of the seasonal forcing? What happens to the periodic solutions in case $\epsilon \rightarrow 0$ and $\epsilon \lesssim 1$?

2 Model derivation

Let $N := S + I$ denote a total host population size on the observed region, which is assumed to be constant due to a relatively tiny increment rate on a usual time scale of the vector dynamics. This population size shares a time-dependent population size of susceptible hosts S and that of passively infective hosts I . Analogously, $M := U + V$ denotes a total vector population size, comprising a population size of susceptible vectors U and that of actively infective vectors V . Our point of departure in the modeling consists in reducing the following SISUV model

$$\begin{aligned} S' &= \mu(N - S) - \tilde{\beta}SV + \gamma I, \\ I' &= \tilde{\beta}SV - (\gamma + \mu)I, \\ U' &= \Lambda - \tilde{\rho}UI - \theta U, \\ V' &= \tilde{\rho}UI - \theta V. \end{aligned} \tag{1}$$

Here, μ denotes the host natural mortality rate, assumed to be the same as the natural natality rate for the sake of the constancy of N . In the vector dynamics, Λ, θ denote the recruitment rate and natural mortality rate, respectively. The parameters $\tilde{\beta}$ and $\tilde{\rho}$ denote the rate of infection from an infective vector to a susceptible human and that from an infective human to a susceptible vector, respectively. The parameter γ denotes the recovery rate that exclusively contains information regarding loss of immunity. As a specific feature of the model, we highlight the dependency of the vector reproduction to the seasonally periodic climatic factors. Taking into account only climatic factors of *commensurable* periods, i.e. those that share rational dependencies, we can model (cf. [6])

$$\Lambda = \xi + \zeta \cos(2\pi\omega t)$$

where $\xi, \zeta, \omega, \omega^{-1}$ denote an intercept, an amplitude, a frequency and the corresponding period, respectively. On the view of the selected climatic factors, ω^{-1} shall be associated with the least common multiple of the commensurable periods. The amplitude ζ serves as a tuning parameter for the importance of seasonality. For the sake of well-posedness and simplicity, we assume that

$$0 \leq \zeta < \xi. \tag{2}$$

Accordingly, the total vector population satisfies

$$M' = \xi + \zeta \cos(2\pi\omega t) - \theta M, \quad M(0) = M_0.$$

The above equation leads to the exact solution

$$M = (M_0 - \bar{M} - \zeta A_c) e^{-\theta t} + \bar{M} + \zeta A_c \cos(2\pi\omega t) + \zeta A_s \sin(2\pi\omega t), \tag{3}$$

where

$$\bar{M} := \frac{\xi}{\theta}, \quad A_c := \frac{\theta}{\theta^2 + 4\pi^2\omega^2}, \quad A_s := \frac{2\pi\omega}{\theta^2 + 4\pi^2\omega^2}. \tag{4}$$

It is clear that the population size converges to a periodic solution as $t \rightarrow \infty$.

For the sake of scaling, we shall divide the host and vector dynamics with reference constants. In the host dynamics, N would be the usual choice. In the vector dynamics, we appoint the average of

M on one full period $[0, \omega^{-1}]$. However, the first term in M as in (3) makes the averaging varying depending on the domain undertaken. Therefore, we restrict M_0 as to satisfy $M_0 - \bar{M} - \zeta A_c = 0$ so that M becomes periodic and yield

$$\omega \int_0^{\omega^{-1}} M(t) dt = \bar{M} \quad \text{and} \quad \omega \int_0^{\omega^{-1}} V(t) dt \leq \bar{M}.$$

The latter holds due to the fact that the nonnegative orthant is invariant under the flow of (1). If seasonality is negligible ($\zeta = 0$), then one yields an identity $M = M_0 = \bar{M}$. We thus define the following scaling

$$\frac{M}{\bar{M}} = 1 + \zeta h(t), \quad \text{where} \quad h(t) := \frac{A_c}{\bar{M}} \cos(2\pi\omega t) + \frac{A_s}{\bar{M}} \sin(2\pi\omega t). \quad (5)$$

It is apparent to see that h is ω^{-1} -periodic. Under the following definitions

$$s := \frac{S}{N}, \quad j := \frac{I}{N}, \quad u := \frac{U}{M}, \quad v := \frac{V}{M}, \quad \beta := \tilde{\beta}\bar{M}, \quad \kappa := \gamma + \mu, \quad \rho := \tilde{\rho}N$$

together with the constancy of N , the system (1) reduces to

$$\begin{aligned} j' &= \beta(1 - j)v - \kappa j, \\ v' &= \rho(1 + \zeta h - v)j - \theta v. \end{aligned} \quad (6)$$

The time scale t in the model (6) is defined on weekly basis.

According to Esteva–Vargas [32], both β and ρ convey entities that lead the contact between host and vector to successful infection. These include the mosquito biting rate and an effectivity measure representing how successful a mosquito bite leads to virus transmission. The former is dependent on hosts' mobility that leads them to sites where the vector population concentrates and how exposed their skins are. The latter is what we can assume to be constant on the population level, even though empirical evidence shows its dependence on age [33]. We assume that most infected hosts are hospitalized, meaning that they are kept in isolated, hygienic rooms where vectors are less likely to present. Consequently, either more hosts are hospitalized or more infective vectors are surrounding hospitals cannot change the mode of mosquito bites to infected hosts. It thus is justifiable to assume that ρ is constant. As far as β is concerned, it is the aim of the current study to model β as a function of the infected host class j , i.e. taking into account the social awareness between susceptible hosts in the observed region. Sections 4–5 are devoted to the corresponding discussions. In what follows, however, a general $\beta = \beta(j)$ apparently affords some preliminary analyses, which will be used in the subsequent sections.

3 Analysis under time scale separation

3.1 Assumptions leading to time scale separation

As a first step we assume that ρ, θ are unobservable. Suppose that data on infected hosts and infected vectors are given, where both fluctuate at certain orders of magnitude, around certain medians (\bar{j}, \bar{v}) . Suppose that θ is pre-specified. On the virtue of data assimilation, ρ can be traced. At this stage, we may assume that the data are not heavily fluctuating, since then $\rho/\theta \approx \bar{v}/(\bar{j}(1 - \bar{v})) = \text{constant}$ due to Euler approximation on v -dynamics in (6) under negligible seasonality ($\zeta = 0$). A large θ in the model returns significant natural deaths, implying smaller vector lifespan, therefore ρ has to be chosen equivalently large to keep the model solution portraying the data. When θ is assigned with a smaller value, or larger vector lifespan, then a smaller force of infection ρ would be preferable to keep the model solution at the same order of magnitude as when using a larger θ . From the system, we deduce that the host and vector lifetime duration fulfil the condition $\mu^{-1} \gg \theta^{-1}$, making both dynamics run on disparate time scales. Accordingly, there exists an *adiabatic parameter* ϵ satisfying

$$0 < \epsilon \ll 1 \quad (7)$$

such that $\theta = \mu/\epsilon$. By such definition, the adiabatic parameter ϵ can also be the *vector–host lifespan ratio*. Since ρ/θ is constant where both ρ and θ are variable, there exists a parameter ρ_ϵ such that $\rho/\theta = \rho_\epsilon/\mu = \rho_\epsilon/(\epsilon\theta)$, implying $\rho_\epsilon = \epsilon\rho$. It is assumed that ρ_ϵ, μ be specified beforehand, while ρ, θ adjust accordingly based on the variation of ϵ . Here we present numerical values of the parameters involved in the model, except where ϵ and ζ vary, satisfying (7) and (2) respectively.

μ^{-1}	γ^{-1}	ρ_ϵ	θ	ρ	ξ	ω^{-1}	\bar{M}	A_c	A_s	M_0
[w]	[w]	[w ⁻¹]	[w ⁻¹]	[w ⁻¹]	[mos. × w ⁻¹]	[w]	[mos.]	[w]	[w]	[mos.]
75×48	24	1.8×10^{-5}	μ/ϵ	ρ_ϵ/ϵ	10^4	52	ξ/θ	$\frac{\theta}{\theta^2 + 4\pi^2\omega^2}$	$\frac{2\pi\omega}{\theta^2 + 4\pi^2\omega^2}$	$M + \zeta A_c$

Table 1: Parameter values and units used in the model simulations.

The appearance of the adiabatic parameter ϵ also rescores the amplitude of the seasonal forcing in the model (6). Let $\text{Ampl}[\cdot]$ denotes the maximal amplitude of a functional argument with periodic behaviour. We get

$$\text{Ampl}[h] = \sqrt{\frac{A_c^2 + A_s^2}{\bar{M}^2}} = \frac{1}{\bar{M}\sqrt{\theta^2 + 4\pi^2\omega^2}} = \frac{\mu}{\xi\epsilon\sqrt{\theta^2 + 4\pi^2\omega^2}},$$

where h is as given in (5). We would thus like to study the possible impact of letting ϵ varying on the periodic solutions emanating from $\zeta > 0$. Further consequence reveals that

$$\text{Ampl}\left[\frac{M}{\bar{M}}\right] = 1 + \zeta \cdot \text{Ampl}[h] = 1 + \left(\frac{\mu}{\xi\sqrt{\theta^2 + 4\pi^2\omega^2}}\right) \left(\frac{\zeta}{\epsilon}\right) \sim \frac{\zeta}{\epsilon}.$$

We see here that the maximal amplitude of the seasonal forcing M/\bar{M} is equivalent to the amplitude ζ , but inversely equivalent to ϵ . As things develop, we will see how the (ζ, ϵ) -variations lead to distinctive maximal amplitudes of not only vector trajectories, but also host trajectories.

3.2 Slow–fast system in the absence of seasonality

The point of departure in the analysis is to see how the autonomous system behaves with respect to the adiabatic parameter ϵ . From the time scale separation, we discover a singularly perturbed system

$$\left. \begin{aligned} j' &= J_0(j) + J_1(j)v \\ \epsilon v' &= V_0(j) + V_1(j)v \end{aligned} \right\} x' = \mathbf{f}(x) = (\mathbf{f}^j, \mathbf{f}^v)(x) \quad (8)$$

where

$$J_0(j) := -\kappa j, \quad J_1(j) := \beta(j) \cdot (1 - j), \quad V_0(j) := \rho_\epsilon j, \quad V_1(j) := -\rho_\epsilon j - \mu,$$

and j, v correspond to the *slow* and *fast dynamics*, respectively. The *critical manifold* of this system is characterized by the curve $(j, v^*(j))_{j \in \mathcal{D}}$ where $v^*(j) = -V_0(j)/V_1(j) = \rho_\epsilon j/(\rho_\epsilon j + \mu)$ and \mathcal{D} is a connected subset of $[0, 1]$. The according slow dynamics should then be governed by $j' = \mathbf{f}^j(j, v^*(j))$ in the critical manifold. This vector field is continuously differentiable with bounded derivative, guaranteeing the existence and uniqueness of j . Since $\partial_v \mathbf{f}^v|_{(j, v^*)} = V_1(j) < 0$, then the critical manifold is *normally hyperbolic* [34] and moreover, asymptotically stable. We use $v \mapsto \mathcal{V}(j, v) : v \mapsto \frac{1}{2}(v - v^*)^2$ for the according Lyapunov function. It is clear that \mathcal{V} has the nondegenerate minimum at the critical manifold, where $\mathcal{V}' = (v - v^*)\mathbf{f}^v/\epsilon = -(\rho_\epsilon j/\epsilon + \mu/\epsilon)(v - v^*)^2 \leq -2(\mu/\epsilon)\mathcal{V}$ owing to $j \in \mathcal{D}$. Due to $0 < \epsilon \ll 1$, there exists a positive constant L where the inequality $\epsilon\mathcal{V}' \leq -2\mu\mathcal{V} + 2\mu L\epsilon\sqrt{\mathcal{V}}$ holds still. Dividing both sides by $2\sqrt{\mathcal{V}}$ and solving the differential inequality forward in time, we obtain the *slaving condition* for the critical manifold

$$|v(t) - v^*(t)| \leq K|v_0 - v_0^*|e^{-\mu t/\epsilon} + L\epsilon, \quad v_0^* = \rho_\epsilon j_0/(\rho_\epsilon j_0 + \mu) \text{ and } K > 0. \quad (9)$$

This shows that the fast dynamics evolve to the critical manifold with respect to the *slow time scale* t . Moreover, at $t = \mathcal{O}(\epsilon|\log \epsilon|)$, any fast dynamics starting from a neighbourhood of order $\mathcal{O}(1)$ of the critical manifold reaches a neighbourhood of order $\mathcal{O}(\epsilon)$ of it. This is in agreement with the standard

result from Tikhonov [35, Theorem 11.1]. Under the slaving condition (9), (t, ϵ) -approximation to the solution of (8) can be calculated using e.g. O'Malley–Vasil'eva expansion [36]. This facilitates an easier way to approximate the solution by dissevering the calculation into those with respect to orders of ϵ .

Here we skip the asymptotic expansions and take a step further. We are instead looking for an intermediate locally attractive manifold, to which all nearby solution trajectories confine, which ultimately coincides with the critical manifold as $\epsilon = 0$. This intermediate manifold is what is known as the *slow manifold*. The fact that the critical manifold is asymptotically stable, Fenichel [37, 38, 39] shows that it perturbs with $\epsilon > 0$ to the slow manifold. We reemploy the slow–fast system (8) and obtain an approximation of v -state in the slow manifold $v = v(j, \epsilon)$ using center manifold analysis around the critical manifold. To do so, we first keep away ϵ from appearing in front of the derivative term by introducing a *fast time scale* $\tau := t/\epsilon$ to the system. Note that, again, t shall be first specified and τ adjusts accordingly. The system is then equivalent to

$$\begin{aligned} j' &= \epsilon (J_0(j) + J_1(j)v), \\ v' &= J_0(j) + J_1(j)v, \\ \epsilon' &= 0. \end{aligned} \tag{10}$$

Now the apostrophe indicates the time derivative with respect to τ . The last system admits the concatenated critical manifold $(j, v^*, 0)$ as its non-hyperbolic equilibrium, i.e. the Jacobian has the eigenvalues $0, \partial_v \mathbf{f}^v|_{(j, v^*)}, 0$. Of course, v^* is the equilibrium of the v -dynamics in (10) and is asymptotically stable due to $\partial_v \mathbf{f}^v|_{(j, v^*)} < 0$. This asymptotic stability of the critical manifold could have never been achieved unless v^* is asymptotically stable in the center manifold. Locally, a slow manifold $(j, v(j, \epsilon), \epsilon)_{(j, \epsilon) \in \mathcal{D}_\epsilon}$, where $\mathcal{D}_\epsilon \subset [0, 1]^2$, acts as a center manifold and the asymptotic stability of the critical manifold makes it locally attractive. According to Center Manifold Theorem, there exists a realization of the slow manifold $v(j, \epsilon) = v^* + \mathcal{O}(\|(j, \epsilon)\|^2)$, which can be written in the following abstraction

$$v(j, \epsilon) = \sum_{i \geq 0} \epsilon^i \mathbf{g}_i(j), \tag{11}$$

where $\mathbf{g}_0 = v^*$. According to either (8) or (10), this ansatz solves the partial differential equation $\mathbf{f}^v = d_\tau v = \partial_j v d_\tau j + \partial_\epsilon v d_\tau \epsilon = \epsilon \partial_j v \mathbf{f}^j$ due to $d_\tau \epsilon = 0$, which is equivalent to

$$V_0 + V_1 v(j, \epsilon) = \epsilon \partial_j v(j, \epsilon) (J_0 + J_1 v(j, \epsilon)). \tag{12}$$

To calculate the slow manifold $v(j, \epsilon)$ numerically, we require to fix ϵ and have certain known point(s) as the initial condition. If $v(j, \epsilon) = v^*(j)$, then the left-hand side of (12) vanishes and the right-hand side of it leaves us either $d_j v^* = 0$, which can never be the case for arbitrary j , or $J_0 + J_1 v^* = 0$. The latter supplements with the fact that the slow manifold intersects with the critical manifold at the equilibria of the slow dynamics. Unfortunately, the only reliable points for the initial conditions are the equilibria, but they give indefinitenesses to start the computation, $\partial_j v = 0/0$. Due to this reason we opt to approximate the slow manifold. The job is done by rearranging (12), whereby

$$-V_0 \epsilon^0 + \sum_{i \geq 0} (-V_1 \mathbf{g}_i) \epsilon^i + \left(J_0 d_j \mathbf{g}_i + \frac{J_1}{2} d_j \sum_{\substack{m, n \geq 0: \\ m+n=i}} \mathbf{g}_m \mathbf{g}_n \right) \epsilon^{i+1} + \left(\frac{J_1}{2} d_j \mathbf{g}_i^2 \right) \epsilon^{2i+1} = 0.$$

At the expense of vanishing all the coefficients of ϵ^i , one further yields

$$0 = -V_0 \delta_{i0} - V_1 \mathbf{g}_i + J_0 d_j \mathbf{g}_{i-1} + \frac{J_1}{2} d_j \sum_{\substack{m, n \geq 0: \\ m+n=i-1}} \mathbf{g}_m \mathbf{g}_n + \frac{J_1}{2} d_j \hat{\mathbf{g}}^2, \quad \text{where } \hat{\mathbf{g}} = \begin{cases} \mathbf{g}_{\frac{i-1}{2}}, & i \text{ odd} \\ 0, & i \text{ even} \end{cases}.$$

We have used δ_{ij} denoting the usual Kronecker delta. This last equation is a linear equation in \mathbf{g}_i whose solution can be calculated straightforward and exhibits a recursion relation. Surely, disclosing

more higher orders is possible but laborious. In the sequel, we will see how solution trajectories of the model approach the slow manifold, before approaching the critical manifold and ultimately approaching stable equilibria of the slow dynamics in the critical manifold. Numerically approximated slow manifolds in the virtue of the above discussion will also be displayed alongside.

3.3 Periodic solutions of the full system

This section presents a check for the existence of ω^{-1} -periodic solutions of (6) under the activation of seasonal forcing $\zeta > 0$, which will be used in the subsequent discussions. The basic idea highlighting the result has been adopted from [40]. Let \hat{x} be an existing equilibrium of the autonomous counterpart $x' = \mathbf{f}(x; \zeta = 0)$. Suppose that we impose an initial condition $x_0 \in U_1(\hat{x})$ for some neighbourhood $U_1(\hat{x})$ and $|\zeta| < \zeta_1$ for some ζ_1 such that a unique solution $x = x(t; x_0, \zeta)$ exists. Now we are looking for an existing periodic solution $x(t; x_0, \zeta)$ surrounding the equilibrium \hat{x} , i.e. $x(t + \omega^{-1}; x_0, \zeta) = x(t; x_0, \zeta)$ for all time $t \geq 0$. This can be rephrased to looking for a suitable ζ -dependent initial condition $x_0(\zeta)$ that leads to the periodic solution. A first step to this, an auxiliary function $S(x_0, \zeta) := x(\omega^{-1}; x_0, \zeta) - x_0$ is set up towards finding $x_0(\zeta)$ that zeros S using Implicit Function Theorem around the point $(\hat{x}, 0)$. Owing to regularity of β , the vector field \mathbf{f} becomes continuously differentiable in time $t \in \mathbb{R}_+$, state $x \in [0, 1] \times \mathbb{R}_+$, and $\zeta \in (-\zeta_1, \zeta_1)$. The function $\partial_{x_0} x(t; \hat{x}, 0)$ satisfies the linear equation

$$d_t \partial_{x_0} x(t; \hat{x}, 0) = \partial_{x_0} \mathbf{f}(x; \zeta)|_{(\hat{x}, 0)} = \partial_x \mathbf{f}(\hat{x}; 0)^\top \partial_{x_0} x(t; \hat{x}, 0), \quad \partial_{x_0} x(0; \hat{x}, 0) = \mathbf{1}.$$

Further linear equation for $\partial_\zeta x$ can also be derived to show that continuity of \mathbf{f} gives continuous differentiability of S on $\mathbb{R}^2 \times (-\zeta_1, \zeta_1)$. It then holds $\partial_{x_0} S(\hat{x}, 0) = \partial_{x_0} x(\omega^{-1}; \hat{x}, 0) - \mathbf{1} = \exp(\partial_x \mathbf{f}(\hat{x}; 0) \omega^{-1}) - \mathbf{1}$. We want to know under which condition this matrix has a bounded inverse. Let v be an eigenvector of $\partial_x \mathbf{f}(\hat{x}; 0)$ that associates with an eigenvalue λ . The Taylor expansion for matrix exponential gives us $(\exp(\partial_x \mathbf{f}(\hat{x}; 0) \omega^{-1}) - \mathbf{1})v = (\exp(\omega^{-1} \lambda) - 1)v$, making $\exp(\omega^{-1} \lambda) - 1$ the associated eigenvalue of $\partial_{x_0} S(\hat{x}, 0)$. It remains to show that for any eigenvalue λ of the Jacobian $\partial_x \mathbf{f}(\hat{x}; 0)$, $\exp(\omega^{-1} \lambda) - 1$ can never be zero or

$$\lambda \neq 2\pi\omega i\mathbb{Z} \tag{13}$$

where i, \mathbb{Z} denote the imaginary number and the set of integers, respectively.

One sufficient condition for the invertibility of $\partial_{x_0} S(\hat{x}, 0)$ is to have a negative trace of the Jacobian. By the Implicit Function Theorem, there exist a domain $U_2(\hat{x}) \times (-\zeta_2, \zeta_2)$ and a continuously differentiable function $x_0(\zeta)$ for which $(\zeta, x_0(\zeta))$ is defined on this domain such that $S(x_0(\zeta), \zeta) = 0$ or eventually $x(\omega^{-1}, x_0(\zeta), \zeta) = x_0(\zeta)$. Since \mathbf{f} is ω^{-1} -periodic over time, then $x(t + \omega^{-1}, x_0(\zeta), \zeta) = x(t, x_0(\zeta), \zeta)$ if and only if $x(\omega^{-1}, x_0(\zeta), \zeta) = x_0(\zeta)$. The desired domain for (x_0, ζ) for the existence of the ω^{-1} -periodic function can then be restricted to $\{U_1(\hat{x}) \cap U_2(\hat{x})\} \times \{(-\zeta_1, \zeta_1) \cap (-\zeta_2, \zeta_2)\}$.

Note that such a negative trace of the Jacobian would give a dissipative autonomous system with the exponential dissipative rate given by the trace, which is another way to see that the autonomous system contracts to a set of measure zero. Added by Dulac–Bendixson’s criterion, the negative trace naturally guarantees non-existence of a limit cycle in the nonnegative quadrant for the autonomous system. When seasonal forcing is activated, this condition prevents the birth of a trajectory where a limit cycle is interfered by such seasonal forcing, i.e. a torus.

3.4 Approximation of periodic solutions

Here we center the investigation on what would be the behaviour of the periodic solutions under variation of the amplitude ζ and adiabatic parameter ϵ . The sinusoidal function $\phi = \zeta h$ where h is as in (5) can be seen as the solution of the differential equation $(\phi', \psi') = (\psi, -4\pi^2 \omega^2 \phi)$ where $(\phi, \psi)(0) = (\zeta A_c / \bar{M}, 2\zeta A_s \pi \omega / \bar{M})$. Under the autonomous setting, the entire system decouples into

$$\begin{aligned} j' &= \beta(j) \cdot (1 - j)v - \kappa j, \\ v' &= \rho(1 + \phi - v)j - \theta v, \\ \phi' &= \psi, \\ \psi' &= -4\pi^2 \omega^2 \phi. \end{aligned} \tag{14}$$

Let (\hat{j}, \hat{v}) denote an equilibrium state of (j, v) -dynamics. The only equilibrium state of (ϕ, ψ) -dynamics is $(\hat{\phi}, \hat{\psi}) = (0, 0)$ with purely imaginary eigenvalues, leading to the fact that any equilibrium of (14) is non-hyperbolic. As an intermediate, let us recall the numerical estimates for observable parameters from Tab. 1 to get an idea of how large ϕ, ψ would be. We apparently obtain

$$\text{Ampl}[\phi] = \zeta \cdot \text{Ampl}[h] = \left(\frac{\mu}{\xi \sqrt{\theta^2 + 4\pi^2 \omega^2}} \right) \left(\frac{\zeta}{\epsilon} \right) \quad \text{and} \quad \text{Ampl}[\psi] = 2\pi\omega \cdot \text{Ampl}[\phi].$$

We also observe from the estimates that $\text{Ampl}[\phi], \text{Ampl}[\psi] \sim \zeta/\epsilon$. Providing that $\epsilon > \mu\zeta/\xi\sqrt{\theta^2 + 4\pi^2\omega^2}$, we can employ Center Manifold Theorem to have a realization of (j, v) -dynamics in the center manifold given by

$$\begin{aligned} j(\phi, \psi) &= \hat{j} + a_1\phi^2 + a_2\phi\psi + a_3\psi^2 + \mathcal{O}(\|(\phi, \psi)\|^3), \\ v(\phi, \psi) &= \hat{v} + b_1\phi^2 + b_2\phi\psi + b_3\psi^2 + \mathcal{O}(\|(\phi, \psi)\|^3). \end{aligned}$$

One can naturally neglect the third-order terms by the preceding estimates of ϕ, ψ . It remains to determine the constants appearing in the ansatz by, instead of proximity optimization, equating j', v' from the actual dynamics and the ansatz as well as focusing solely on small-order terms:

$$\begin{aligned} j' &= (2a_1\phi + a_2\psi)\psi + (2a_3\psi + a_2\phi)(-4\pi^2\omega^2\phi) = \beta(j) \cdot (1 - j)v - \kappa j|_{j(\phi, \psi), v(\phi, \psi)}, \\ v' &= (2b_1\phi + b_2\psi)\psi + (2b_3\psi + b_2\phi)(-4\pi^2\omega^2\phi) = \rho(1 + \phi - v)j - \theta v|_{j(\phi, \psi), v(\phi, \psi)}. \end{aligned}$$

Depending on how complicated β is, the computations of the constants can get laborious. Prominent from this investigation is that the periodic ansatz of j, v in the center manifold perturb from the equilibrium states \hat{j}, \hat{v} with sinusoidal functions of amplitudes equivalent to $(\zeta/\epsilon)^2$ in case $\epsilon > \mu\zeta/\xi\sqrt{\theta^2 + 4\pi^2\omega^2}$. In case $\epsilon \leq \mu\zeta/\xi\sqrt{\theta^2 + 4\pi^2\omega^2}$, the higher orders in the center manifold approximation matter and ϵ takes the lead in extending the amplitude. Therefore, no small-order polynomial approximation of the periodic solutions can be envisaged. A crude estimate on the vector lifespan $\theta^{-1} \approx 4w$ gives $\epsilon = \mu/\theta = 4\mu \geq 4\mu\zeta/\xi > \mu\zeta/\xi\sqrt{\theta^2 + 4\pi^2\omega^2} \approx 3.6\mu\zeta/\xi$, suggesting that the second-order approximation is already quite reasonable. The preceding exposition gives us a new tool in designing the model to have periodic solutions that will correct the assimilation to given data. In Section 3.1, the solution of the autonomous model was deduced to portray lightly fluctiative data irrespective of ϵ . In case the seasonal forcing is activated, we can make use of both ζ and ϵ to create an amplitude that delineates that of the data. Questionable is thus how to correctly specify the numerical value of ρ_ϵ . We have just foreseen the use of the model for data assimilation under specification of three unobservable parameters.

4 When hospitals can accommodate an unlimited number of patients

Note, first of all, that both j and I can be treated equally in the modeling since j is linearly proportional to I . In such case, we can directly initiate models of the infection rate β as a function of j . Suppose that in the absence of disease, $j = 0$, the introduction of infective vector population gives rise to a certain driving force, represented by the initial infection rate β_0 . We suppose that β stays more-or-less constant while the hosts are still unaware of the ongoing infections, then initiates decrement around a certain reference point $j^* \in [0, 1)$. This threshold j^* indicates the alarming incidence level under which medical departments can never transfer information to media holders for either time, interest or financial restrictions. The interval on which such driving force decreases, i.e. $j^* \leq j$, is that when the humans stay alarmed of the ever increasing infections, i.e. where self-precautions and hospitalizations are urgently undertaken. Of course, such awareness can never be achieved unless the media keep reporting on current infection cases. When j increases further, a slow downturn in the infection rate is assigned due to fewer contacts between hosts and vectors. When j is close to the maximum ($j = 1$), β saturates to a certain level $\beta_1 < \beta_0$, since most of the hosts are aware of the danger and to be equipped with uniform self-defence system, also many of them are hospitalized. The preceding description leads us to the following summary on β :

(A1) $\beta(j) > 0$ for all $j \in [0, 1]$,

(A2) $\beta_0 = \beta(0) > \beta(1) = \beta_1$,

(A3) $\beta'(j) = 0$ for $j \in [0, j^*]$ and $\beta'(j) < 0$ for all $j \in (j^*, 1]$.

The slow dynamics j in the critical manifold are governed by

$$j' = J_0(j) + J_1(j)v^*(j) = \beta(j) \cdot (1-j) \frac{\rho_\epsilon j}{\rho_\epsilon j + \mu} - \kappa j. \quad (15)$$

We know that $[0, 1]$ is invariant due to the boundary conditions $j'(0) = 0$ and $j'(1) < 0$. At the end of Section 3.2, we came into understanding that whichever equilibrium of (15) should be where the critical and slow manifold intersect. The equation (15) has the trivial equilibrium, known as *disease-free equilibrium*, $j = 0$. It is instantly verifiable that the Jacobian $d_j j'|_{j=0} = \beta_0 \rho_\epsilon / \mu - \kappa = \kappa(\beta_0 \rho_\epsilon / \mu \kappa - 1) < 0$, providing that the *basic reproductive number*

$$\mathcal{R}_0 := \sqrt{\beta_0 \rho_\epsilon / \mu \kappa} < 1. \quad (16)$$

At this point, we acquire local asymptotic stability of $j = 0$. If $\mathcal{R}_0 > 1$, then $j = 0$ is unstable. If $\mathcal{R}_0 = 1$, then one can take a small $\varepsilon > 0$ and easily verify that $j'j|_{j=\varepsilon} = -(\kappa + \beta(\varepsilon))\varepsilon^2 + \beta(\varepsilon)\varepsilon > 0$ due to $\lim_{\varepsilon \rightarrow 0^+} \beta(\varepsilon)\varepsilon / (\kappa + \beta(\varepsilon))\varepsilon^2 = \beta_0 / (\kappa + \beta_0) \lim_{\varepsilon \rightarrow 0^+} 1/\varepsilon = \infty$. This indicates that $j = 0$ is repelling in the positive real.

Calculating a nontrivial solution, i.e. *endemic equilibrium*, is quite straightforward. Factoring out j from (15), we are in the position to solve

$$E(j) := \beta(j) \cdot (1-j)\rho_\epsilon - \kappa(\rho_\epsilon j + \mu) = 0. \quad (17)$$

Observe that $E(0) = \beta_0 \rho_\epsilon - \mu \kappa = \mu \kappa (\mathcal{R}_0^2 - 1)$, $E(1) = -\kappa(\rho_\epsilon + \mu) < 0$ and $E'(j) = \beta'(j) \cdot (1-j)\rho_\epsilon - \beta(j) \cdot \rho_\epsilon - \kappa \rho_\epsilon < 0$ for all $j \in (0, 1]$ due to (A1)–(A3). We acquire a dichotomy. If $\mathcal{R}_0 \leq 1$, then there exists no endemic equilibrium. If $\mathcal{R}_0 > 1$, then there exists a unique endemic equilibrium $j = j_e \in (0, 1)$ approaching the disease-free equilibrium as $\mathcal{R}_0 \rightarrow 1^+$, i.e. due to fixed $E(1)$. Furthermore, as we calculate the Jacobian, it turns out to be

$$d_j j'|_{j=j_e} = d_j \frac{E(j) \cdot j}{(\rho_\epsilon j + \mu)} \Big|_{j=j_e} = \frac{E'(j) \cdot j}{(\rho_\epsilon j + \mu)} + E(j) \cdot \frac{\mu}{(\rho_\epsilon j + \mu)^2} \Big|_{j=j_e} = \frac{E'(j_e) \cdot j_e}{(\rho_\epsilon j_e + \mu)} \quad (18)$$

such that

$$\text{sign} \left(d_j j'|_{j=j_e} \right) = \text{sign}(E'(j_e)). \quad (19)$$

Additionally attributed to $\mathcal{R}_0 > 1$ is thus the local asymptotic stability of the endemic equilibrium. After all, the preceding exposition shows that the slow dynamics using β fulfilling (A1)–(A3) exhibits a supercritical bifurcation at $\mathcal{R}_0 = 1$. Note that the bifurcation profile cannot change with the adiabatic parameter ϵ due to \mathcal{R}_0 's independency on it. Moreover, the similar bifurcation would appear in case β is strictly monotonically decreasing. This stems from the simple fact that the analysis is independent on j^* , i.e. that one can thus set $j^* = 0$ in (A3). Similar results of supercritical bifurcation with respect to \mathcal{R}_0 using non-increasing β can also be seen in [15].

As $\epsilon > 0$, we still keep the full system (6) on our hand. Apparently, the Jacobians evaluated at the disease-free equilibrium $(0, 0)$ and endemic equilibrium (j_e, v_e) with $v_e = v^*(j_e)$ have the traces

$$-\beta_0 v_e - \kappa - \theta \quad \text{and} \quad \beta'(j_e) \cdot (1-j_e)v_e - \beta(j_e) \cdot v_e - \kappa - \rho j_e - \theta$$

respectively, which are clearly negative. One can thus not expect to have purely imaginary eigenvalues for each Jacobian, fulfilling the existence check (13). A closing statement in this section is that there always exist ω^{-1} -periodic solutions surrounding the equilibria.

5 Limited medical access and the increase of infection rate

Here we consider a scenario where the available hospitals in the observed region can only accommodate a certain population share $j^* \in [0, 1)$. As such, the alarming incidence level j^* gains a new definition. We consider a setting where no reports to the media are initiated in case hospitals still manage to shelter patients. Unawareness of the susceptible hosts for the case $j \leq j^*$ thus leads to a constant $\beta = \beta_0$. A decrement in β happens when the media keep reporting not only the current endemicity, but also the absence of medical access. The phase, in which case a sudden decrement in the infection rate happens, is what we consider as that when susceptible hosts *overreact* to the advancing disease propagation and that there is nowhere to go for cure.

Let us now consider a situation where the investigated vector-borne disease is endemic in a developing region. By developing we point at the human tendency of disobeying regulations towards healthy life and inability as well as unwillingness to regularly afford household's preventive medicines. It is also ubiquitous that developing regions be identical with "population explosion" and limited medical access. The fact that vector-borne diseases, such as dengue, are endemic in areas of relatively hot temperature and high air humidity that befit well with vector breeding, the concepts of putting on full-cover clothing and smearing repellent fluids sound counter-intuitive. Other measures such as disseminating *temephos*, cleaning household vessels, and fumigation usually go on individual basis and require a big campaign for the effectivity in a population scale [41]. The fact that disease vectors, such as *Aedes aegypti* mosquitoes, only bite during daylight also makes such small self-defence measures prone to discontinuation. Despite high awareness about the disease and preventive measures, a study has shown that typical vector-borne disease with a low case-fatality rate is perceived deadly by only a portion of susceptible humans, while others perceive it easily curable [42]. Here we consider the situation where β revolves in the likelihood of disowning preventive measures, absence of hospitals, poverty, and perceiving the disease of being easily curable. A prominent psychological trigger can be seeing through increasing incidences in the neighbourhood with despair, as continuous usage of preventive measures can seemingly not suppress the incidence level. Another unforeseeable phenomenon when j increases further, such that the estimate of mosquito population $v^*(j)$ also increases, is that the susceptible humans are evermore surrounded by hungrier vectors [43]. This surely gives additional correction to β for sufficiently large j . In summary, we consider β that satisfies:

$$(B1) \quad \beta(j) > 0 \text{ for all } j \in [0, 1],$$

$$(B2) \quad \beta'(j) = 0 \text{ for } j \in [0, j^*] \text{ with } \beta(0) = \beta_0 \text{ and } \beta'(j) < 0 \text{ for all } j \in (j^*, c] \text{ for a certain positive } c < 1,$$

$$(B3) \quad \beta'(j) > 0 \text{ for all } j \in (c, 1] \text{ and slowly saturates to } \beta(1) = \beta_1.$$

Based on the preceding specifications, we propose the following ansatz

$$\beta(j) := a + \frac{b|j - c|}{d + |j - j^*|}$$

for some constants a, b, c, d . Relying on (B2), we can compute b, d to have

$$\beta(j) := a + \frac{(\beta_0 - a)|j - c|}{c - j^* + |j - j^*|}. \quad (20)$$

This formula clearly produces spikes at j^* and c . The parameter a represents the minimum value of β , which is attained at c . This definition also means $\beta_0 \geq a$. Moreover, there are several ways to treat β as to study bifurcation. The basic idea is to keep some parameters fixed, while others vary. Since we look further upon the variation of equilibria with respect to that of the basic reproductive number, varying β_0 shall do the job. We additionally assume that a, j^* and c are observable, leading to the variation of β_1 as β_0 varies. This way also provides flexibility in to which level β ultimately increases when j gets larger. Further analysis also shows that $1 - c < 1 - j^*$, leading to $\beta_1 < \beta_0$ for all possible choices of β_0 . Finally, the realization of β for a certain set of parameters can be seen in Fig. 1. There we have classified the domain $[0, 1]$ into three regimes based on the value of the incidence level j .

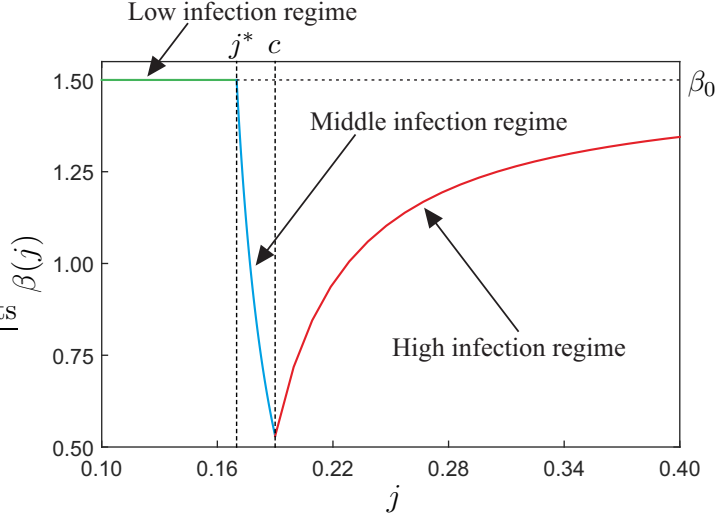


Figure 1: Behavior of the infection rate considering media reporting and several factors persuading increment for larger j . The curve is computed for $a = 0.53$, $\beta_0 = 1.5$, $j^* = 0.17$ and $c = 0.19$, see (20). The infection rate defines three operation modes: low infection regime ($j \leq j^*$), middle infection regime ($j^* < j \leq c$) and high infection regime ($j > c$).

As far as the slow dynamics j in the critical manifold is concerned, we still get from (15) using β in (20) the disease-free equilibrium $j = 0$. The same investigation over the Jacobian $d_j j'$ shows local asymptotic stability of the equilibrium in case $\mathcal{R}_0 < 1$ and instability in case $\mathcal{R}_0 \geq 1$.

Now let us analyze the existence of endemic equilibria. The most important insights from the formulation of β in (20) are that $\beta \rightarrow \beta_0$ as $j^* \rightarrow c^-$ and that $\beta < \beta_0$ as $c > j^*$. Let us recall the function E in (17) for the purpose of finding endemic equilibria. The entities $E(0) = \mu\kappa(\mathcal{R}_0^2 - 1)$ and $E(1) = -\kappa(\rho_\epsilon + \mu) < 0$ remain unchanged. The aforementioned insights further reveal that E is bounded above by a linear function in j , i.e.

$$E(j) \leq \beta_0(1 - j)\rho_\epsilon - \kappa(\rho_\epsilon j + \mu) = -(\beta_0\rho_\epsilon + \kappa\rho_\epsilon)j + E(0) \quad \text{for all } j \in [0, 1],$$

where the equality holds for $c = j^*$. With this finding, the existence analysis becomes much simple. If $\mathcal{R}_0 \leq 1$, then $E(0) \leq 0$ and E can never have roots in $(0, 1]$, therefore no endemic equilibrium is prevailing. For the sake of further analysis, let us reveal

$$E(j^*) = \frac{\rho_\epsilon(2 + c - 3j^*)}{c - j^*}\beta_0 - \rho_\epsilon \frac{2a(1 - j^*)}{c - j^*} - \rho_\epsilon(\kappa + 2a). \quad (21)$$

If $\mathcal{R}_0 > 1$, we can consider two cases: $E(j^*) \leq 0$ and $E(j^*) > 0$, each of which is dependent on β_0 . The former gives the existence of a unique endemic equilibrium in $(0, j^*]$, which is locally asymptotically stable due to $E' < 0, E = 0$ at that point, see (19). The latter case $E(j^*) > 0$ requires information on $E(c) = a(1 - c)\rho_\epsilon - \kappa(c\rho_\epsilon + \mu)$, which is surely greater than $E(1)$. When $E(c) > 0$, we have the existence of a unique endemic equilibrium in $(c, 1)$, which is also locally asymptotically stable. When $E(c) = 0$, we need to check the shape of E on $(c, 1]$ in order to estimate the other endemic equilibria therein. We found that

$$E'(c^+) = \frac{\rho_\epsilon(1 - c)}{2(c - j^*)}\beta_0 - a\rho_\epsilon \frac{1 - j^*}{2(c - j^*)} - \rho_\epsilon(a + 2\kappa), \quad (22)$$

$$E''(j) = \frac{-4\rho(\beta_0 - a)(c - j^*)(1 + c - 2j^*)}{(j + c - 2j^*)^3} < 0 \quad \text{for all } j \in (c, 1] \quad (23)$$

in case $c > j^*$. The second result indicates that E is concave on $(c, 1]$. We see that two endemic equilibria can exist in case β_0 makes $E'(c^+) > 0$. Suppose that this is indeed the case. We naturally lose the information regarding the stability of $j = c$ due to non-uniqueness of $E'(c)$ due to the non-unique subgradients. The other equilibrium in $(c, 1)$ surely is locally asymptotically stable because of $E' < 0$.

The last case $E(c) < 0$ gives a unique endemic equilibrium in (j^*, c) , which is, again, locally asymptotically stable due to (19). From (21) and (22), we come to understand that β_0 acts to “pull” the curve of E towards positivity on $(c, 1]$, until then the curve delineates the decreasing straight line as E devolves. Therefore, depending on how close c and j^* are and how large β_0 is, we can have either none, one, or two more endemic equilibria in $(c, 1)$. In case one endemic equilibrium is found in $(c, 1)$, it should be equipped with $E = E' = 0$, which leads us to unknown status regarding its stability. In case two endemic equilibria are found, it thus is obvious that the smaller one is unstable, while the larger one is locally asymptotically stable due to (19). Another obviousness is that the equilibrium in (j^*, c) and the smaller equilibrium in $(c, 1)$ become closer to each other as j^* and c get closer. As far as $E(c) < 0$ is concerned, we can derive a sufficient condition such as $a \leq \kappa c / (1 - c)$ that will lead to it, where more certainty can be gained as c walks towards 1.

We are now analyzing the existence of periodic solutions surrounding the existing equilibria. Suppose that $\zeta > 0$ and $\epsilon > 0$. Let (\hat{j}, \hat{v}) be an equilibrium of the full system where $\hat{v} = v^*(\hat{j})$. The Jacobian of the system evaluated at the equilibrium in terms of the function E takes the form

$$\partial_x \mathbf{f}(\hat{x}; 0) = \begin{pmatrix} \frac{1}{\rho \epsilon \hat{j} + \mu} (E'(\hat{j})\hat{j} - \kappa\mu) & \beta(\hat{j}) \cdot (1 - \hat{j}) \\ \rho(1 - \hat{v}) & -\rho\hat{j} - \theta \end{pmatrix}. \quad (24)$$

Suppose that β_0 is large enough such that four equilibria are present. When $\hat{j} = 0$, one can easily verify that the trace of the Jacobian is negative, avoiding having purely imaginary eigenvalues. Therefore, a ω^{-1} -periodic solution surrounding the disease-free equilibrium $(0, 0)$ exists, which turns to be the equilibrium itself. One can easily verify this by the fact that the disease-free equilibrium solves the non-autonomous model irrespective to the values of ζ . The endemic equilibria corresponding to the smallest and largest \hat{j} were shown to fulfill $E'(\hat{j}) < 0$, making the trace of the Jacobian negative. This evidence, once again, shows that ω^{-1} -periodic solutions surrounding the two endemic equilibria exist. The equilibrium corresponding to \hat{j} in between the other two endemic equilibria discovers $E'(\hat{j}) > 0$. Variation in $E'(\hat{j})\hat{j} - \kappa\mu$ can thus make the trace obtain either a negative, zero, or a positive value. In case the trace is zero, then $E'(\hat{j})\hat{j} - \kappa\mu$ must have been positively large enough, but then the determinant of the Jacobian becomes negative. We acquire two real roots of the same absolute value that solely oppose in sign. Therefore, a ω^{-1} -periodic solution surrounding this middle endemic equilibrium also exists.

6 Numerical analysis of the model via path-following methods

The epidemic model considering the infection rate introduced in the previous section can be studied in the framework of *piecewise-smooth dynamical systems* [44]. This type of systems arises typically when some kind of nonsmooth phenomenon is considered, such as (soft) impacts, switches, friction, etc. The system response in this case is determined by a piecewise-smooth vector field due to the presence of discrete events producing discontinuities in first or higher-order derivatives of the solution. In our epidemic model, the nonsmoothness is produced by sharp transitions in the force of infection due to the social behavior towards media reports as well as poverty and reluctance in applying measures against the spread of the disease.

In general, a piecewise-smooth dynamical system can be defined in terms of two main components: a collection of (smooth) vector fields and *event functions*. In this way, the system is characterized by a number of operation modes, each of which is associated with a specific smooth vector field. On the other hand, the event functions define the boundary for the operation modes, in such a way that whenever the solution crosses transversally a certain boundary defined by (usually the zero-set of) an event function, the system changes to a different operation mode governed by a (possibly) different vector field. In this way, any solution of the piecewise-smooth dynamical system can be represented by a sequence of *segments*, which consists of a pair given by a smooth vector field describing the model behavior and an event function that defines the terminal condition for the operation mode. More details about this formulation can be found in [45, 46].

6.1 Mathematical setup

For the numerical study of the underlying epidemic model via continuation methods, it is convenient to write the governing equations in autonomous form. To do so, we will consider the following nonlinear oscillator that will be appended to the system [47]:

$$\begin{cases} p' = p + 2\pi\omega q - p(p^2 + q^2), \\ q' = q - 2\pi\omega p - q(p^2 + q^2), \end{cases} \quad (25)$$

with the asymptotically stable solution $p(t) = \sin(2\pi\omega t)$ and $q(t) = \cos(2\pi\omega t)$. In this way, we can write the periodically forced system (6) in the autonomous setting, which then allows us to study the model via numerical continuation methods. Let us define $\alpha := (\beta_0, a, j^*, c, \kappa, \mu, \epsilon, \rho_\epsilon, \xi, \omega, \zeta) \in (\mathbb{R}^+)^{10} \times \mathbb{R}_0^+$ and $z(t) := (j(t), v(t), p(t), q(t)) \in (\mathbb{R}_0^+)^2 \times \mathbb{R}^2$ as the parameters and state variables of the system, respectively, where \mathbb{R}_0^+ stands for the set of nonnegative real numbers. As explained above, any solution of the considered Dengue epidemic model can be divided into the following segments (see also Fig. 1).

Low infection regime. This segment occurs when the incidence level is low (i.e. $j \leq j^*$). Therefore, the media do not apprise susceptible hosts of such a state. Emanating from (6) coupled with the seasonal forcing, the model behavior during this regime is governed by the (smooth) ordinary differential equation

$$z' = \mathbf{f}_{\text{LI}}(z, \alpha) := \begin{pmatrix} \beta_0(1-j)v - \kappa j \\ \frac{\rho_\epsilon}{\epsilon} \left(1 + \frac{\zeta A_\epsilon}{M} q + \frac{\zeta A_s}{M} p - v \right) j - \frac{\mu}{\epsilon} v \\ p + 2\pi\omega q - p(p^2 + q^2) \\ q - 2\pi\omega p - q(p^2 + q^2) \end{pmatrix}. \quad (26)$$

This segment terminates when the incidence level increases beyond j^* , which can be detected via the *event function* $h_1(z(t), \alpha) := j(t) - j^* = 0$. In this case, the system switches to the operation regime given below.

Middle infection regime. During this operation mode, the incidence level lies in the window $j^* < j \leq c$, where the hospitals cannot accept more patients and appeal for regular reports eventually made by the media. As a result of *overreaction*, the rest of susceptible hosts forcefully mobilize everything to keep them on the safe zone. This has then the effect of decreasing the force of infection, thus eventually decreasing the infection rate (see Fig. 1). During this regime, the model obeys the following equation

$$z' = \mathbf{f}_{\text{MI}}(z, \alpha) := \begin{pmatrix} \left(a - \frac{(\beta_0 - a)(j - c)}{j + c - 2j^*} \right) (1-j)v - \kappa j \\ \frac{\rho_\epsilon}{\epsilon} \left(1 + \frac{\zeta A_\epsilon}{M} q + \frac{\zeta A_s}{M} p - v \right) j - \frac{\mu}{\epsilon} v \\ p + 2\pi\omega q - p(p^2 + q^2) \\ q - 2\pi\omega p - q(p^2 + q^2) \end{pmatrix}. \quad (27)$$

This regime terminates in two ways. First, the incidence level decreases below j^* , in which case $h_1(z(t), \alpha) = 0$. Consequently, the system switches back to the low infection regime defined above. Second, the incidence level increases beyond c , which can be detected via the vanishing *event function* $h_2(z(t), \alpha) := j(t) - c = 0$. If this occurs, then the system operates under the regime defined next.

High infection regime. This regime certifies the increasing infection rate with the incidence level $j > c$ (see Fig. 1). The hypothetical causes were due to poverty, hungrier vectors, absence of medical access, reluctance in regularly taking up preventive measures, and despair caused by long lasting high levels of incidences despite keeping up caution. The model behavior during this regime

then obeys the equation

$$z' = \mathbf{f}_{\text{HI}}(z, \alpha) := \begin{pmatrix} \left(a + \frac{(\beta_0 - a)(j - c)}{j + c - 2j^*} \right) (1 - j)v - \kappa j \\ \frac{\rho\epsilon}{\epsilon} \left(1 + \frac{\zeta A_e}{M} q + \frac{\zeta A_s}{M} p - v \right) j - \frac{\mu}{\epsilon} v \\ p + 2\pi\omega q - p(p^2 + q^2) \\ q - 2\pi\omega p - q(p^2 + q^2) \end{pmatrix}. \quad (28)$$

This segment terminates when the level of incidences decreases below c (i.e. $h_2(z(t), \alpha) = 0$), in such a way that the system operates then under the middle infection regime defined above.

Under this setting, the epidemic model introduced in the previous section can be written as a piecewise-smooth dynamical system as follows

$$\begin{cases} z' = \mathbf{f}_{\text{LI}}(z, \alpha), & j \leq j^* \quad (\text{low infection regime}), \\ z' = \mathbf{f}_{\text{MI}}(z, \alpha), & j^* < j \leq c \quad (\text{middle infection regime}), \\ z' = \mathbf{f}_{\text{HI}}(z, \alpha), & j > c \quad (\text{high infection regime}). \end{cases} \quad (29)$$

6.2 Numerical investigation of the epidemic model subject to one-parameter variations

In this section, our main goal is to study the behavior of the model (29) when selected parameters are varied. For this purpose, we introduce a solution measure in order to interpret the numerical results in the context of the considered epidemiological scenario. Suppose that (j, v, p, q) is a bounded periodic solution of system (29) with the fundamental period ω^{-1} . Under this assumption, we define the following solution measure

$$j_{\max} := \max_{0 \leq t \leq \omega^{-1}} j(t), \quad (30)$$

which gives the peak of incidence level within the time window $[0, \omega^{-1}]$. Therefore, one of the main concerns is to investigate under what conditions j_{\max} can be kept as low as possible. In addition, we consider the solution measure

$$j_{\text{p}} := \max_{0 \leq t \leq \omega^{-1}} j(t) - \min_{0 \leq t \leq \omega^{-1}} j(t), \quad (31)$$

which gives the peak-to-peak amplitude of the j -component of the periodic solution.

To analyze the behavior of the model (29), we employ path-following (numerical continuation) methods for piecewise-smooth dynamical systems. Numerical continuation is a well-established approach for comprehensive investigation of a model dynamics subject to parameter variations [47], with particular focus on the detection of parameter values for which the system behavior suffers significant changes (bifurcations). In the present work, we employ the continuation software COCO (Computational Continuation Core [46]), a versatile development and analysis platform oriented to the numerical treatment of continuation problems solved via MATLAB. In particular, we will make extensive use of the COCO-toolbox ‘hspo’, which implements a set of numerical routines for the path-following and bifurcation study of periodic orbits of piecewise-smooth dynamical systems.

The point of departure for the numerical study is the periodic solution shown in Fig. 2(a) (inner diagram), whereas previous sections solely afford the study on their existence, not the stability. The periodic solutions are hereby computed for the parameter values given in Tab. 1. Via one-parameter continuation, we investigate how this solution is affected by the amplitude of the seasonal forcing ζ (see (2)). The corresponding result is shown in Fig. 2, which presents the behavior of the peak of incidence level j_{\max} with respect to ζ . As analytically foreseen in Section 3.4, the peak of incidence level grows with ζ . Note that larger ζ means higher seasonal variation of the vector population due to meteorological factors (humidity, rainfall, temperature, etc.). As explained in Section 6.1, the model (29) belongs to the class of piecewise-smooth dynamical systems, which, in contrast to smooth dynamical systems, can undergo the so-called *grazing* bifurcation [44]. It occurs when a limit cycle makes (quadratic) tangential contact with a discontinuity boundary, defined by an event function

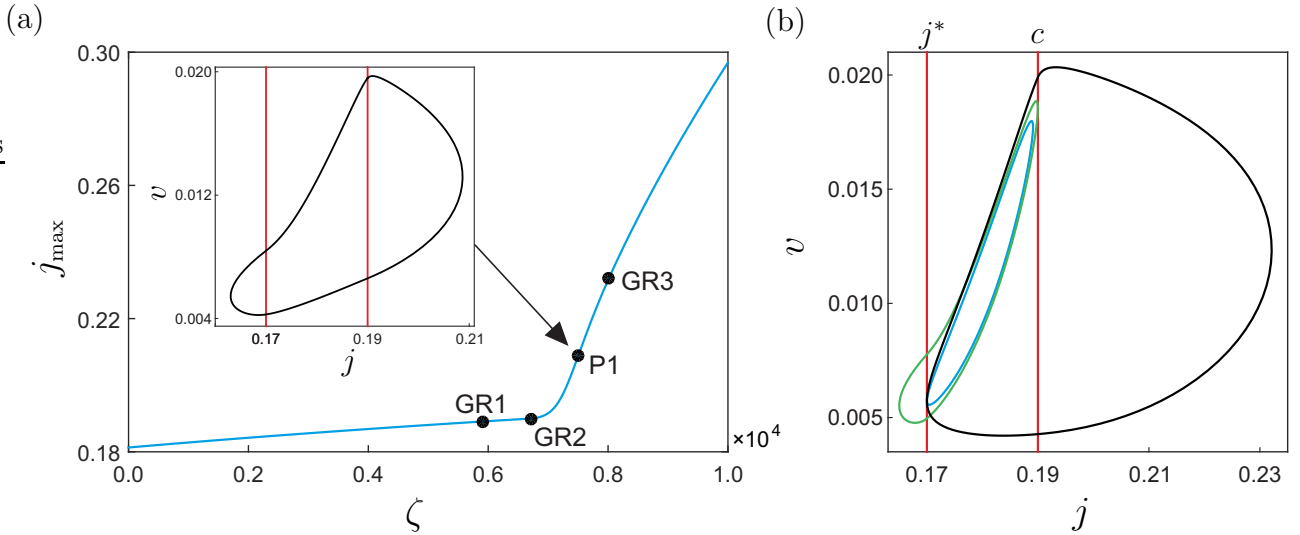


Figure 2: One-parameter continuation of the periodic response shown in panel (a) (inner diagram) with respect to the amplitude of seasonality effects ζ , for the parameter values given in Table 1, with $a = 0.53$, $\beta_0 = 1.5$, $j^* = 0.17$, $c = 0.19$ and $\epsilon = 9.8 \times 10^{-4}$. The left panel depicts the behavior of the peak of incidence level j_{\max} (see (30)) as the parameter ζ varies. The labels $\text{GR}i$ stand for grazing solutions shown in panel (b) ($\text{GR}1$ in blue, $\text{GR}2$ in green, $\text{GR}3$ in black), while the point $\text{P}1$ marks the initial periodic solution taken at $\zeta = 7500$. Vertical red lines in the phase plots stand for the discontinuity boundaries defined at $j = j^*$ and $j = c$.

introduced in Section 6.1. In our case, there are two discontinuity boundaries, given at $j = j^*$ and $j = c$. Consequently, during our investigation we found three grazing bifurcations, located at $\zeta \approx 5.9192 \times 10^3$ ($\text{GR}1$), $\zeta \approx 6.7175 \times 10^3$ ($\text{GR}2$) and $\zeta \approx 8.0143 \times 10^3$ ($\text{GR}3$). Phase plots of the corresponding grazing periodic solutions are depicted in Fig. 2(b), where the tangential intersections with the discontinuity boundaries can clearly be seen. A remarkable feature of the bifurcation diagram shown in Fig. 2(a) is the strong growth of the peak after the grazing bifurcation $\text{GR}2$. This phenomenon is produced precisely due to the crossing of the solution through the boundary $j = c$, after which it is assumed that the impact of media vanishes or the information has become tediously irrelevant for the susceptible subpopulation, and therefore the force of infection increases rapidly (see Fig. 1).

Let us now investigate the behavior of the model (29) when β_0 (see (20) and Fig. 1) varies. The response curve can be seen in Fig. 3(a). To discuss the obtained result, let us begin from the left part of the diagram, where β_0 is small. If this is the case, the system presents an asymptotically stable disease-free equilibrium represented by the solid red line. This means that the incidence level among the population will decrease in time until it disappears (for $t \rightarrow \infty$). During this regime, we have that $\mathcal{R}_0 < 1$ (see (16)). When \mathcal{R}_0 becomes larger than one (at $\beta_0 \approx 0.6473$), the disease-free equilibrium loses stability, and a branch of endemic periodic solutions is born. The latter gives rise to a branching point labeled BP (see Fig. 3(b)). Note that after this BP point, a significant increment of the peak of incidence level can be observed, until the grazing bifurcation $\text{GR}1$ ($\beta_0 \approx 0.7795$) is found. This is then followed by a sluggish increment of the endemic equilibrium state. The reason behind is because after the bifurcation point $\text{GR}1$ (where the periodic solution makes a tangential contact with the discontinuity boundary $j = j^*$ from below), the solution crosses the threshold $j = j^*$, at which it is assumed that the media give regular reports about the disease spread among the susceptible population. Therefore, people take preventive measures in such a way that the infection rate decreases significantly (see Fig. 1). If β_0 grows further, two additional grazing points are found at $\beta_0 \approx 1.1624$ ($\text{GR}2$, grazing contact with $j = c$) and $\beta_0 \approx 1.5837$ ($\text{GR}3$, grazing contact with $j = j^*$ from above). For larger β_0 , a *fold* bifurcation happening at the fold point $\text{F}1$ ($\beta_0 \approx 1.7757$) is detected, where the periodic solution becomes unstable. This unstable periodic response undergoes another grazing bifurcation at $\beta_0 \approx 1.6660$ ($\text{GR}4$, grazing contact with $j = c$) and recovers stability at the fold point $\text{F}2$ ($\beta_0 \approx 1.1494$). After this point, the solution remains stable with the increasing peak of incidence level as β_0 gets larger.

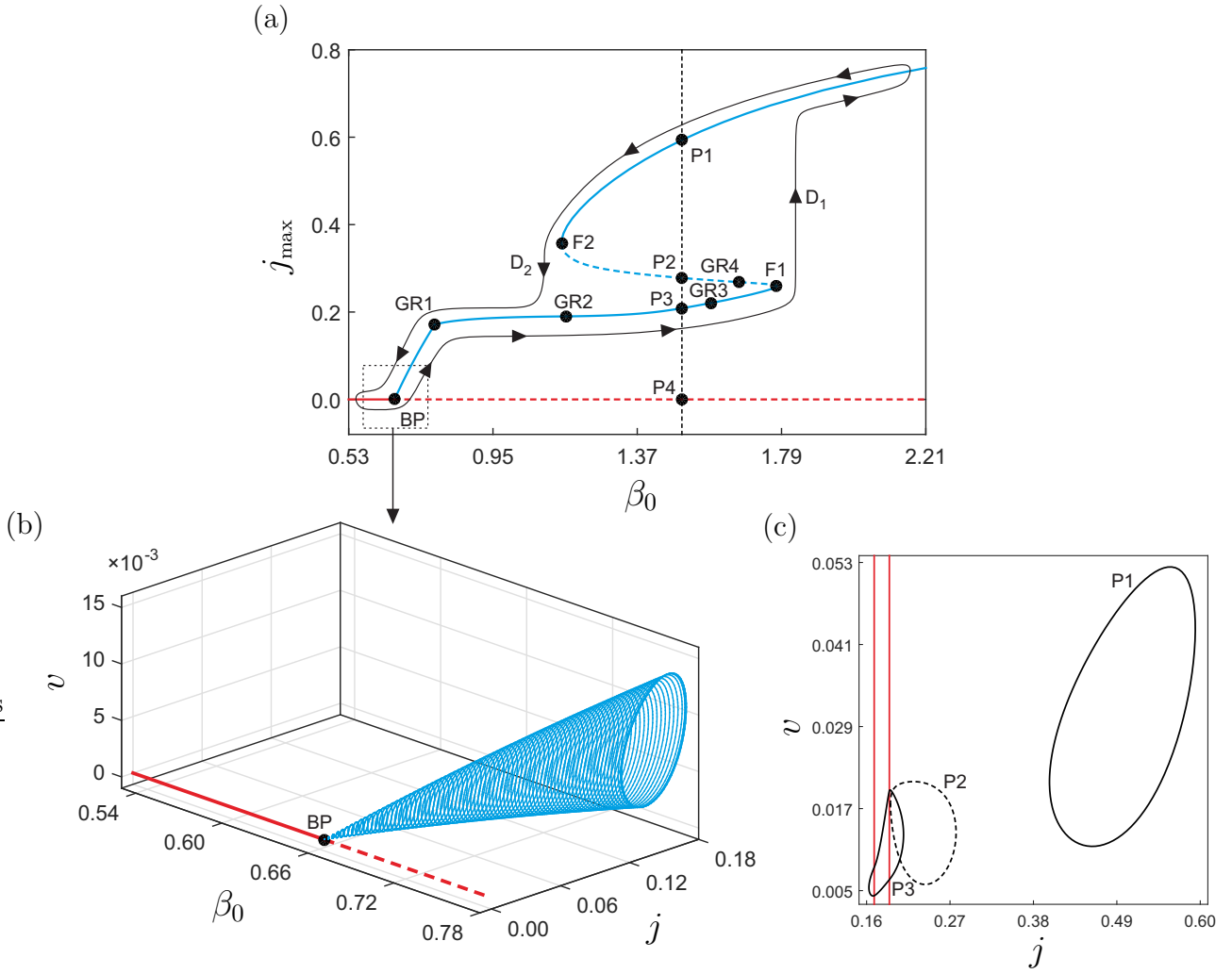


Figure 3: (a) One-parameter continuation of the periodic response shown in Fig. 2(a) with respect to β_0 (see (20)). In this diagram, the blue curve represents continuation of periodic solutions, while the red line stands for continuation of the disease-free equilibria. Solid and dashed lines depict stable and unstable solutions, respectively. The labels BP, F_i and GR_i represent a branching point, fold and grazing bifurcations of limit cycles, respectively, while the labels P_i correspond to coexisting solutions found for $\beta_0 = 1.5$ (see panel (c)). The closed curve D_1 – D_2 represents schematically a hysteresis loop of the system. Panel (b) shows the solution manifold computed during the one-parameter continuation around the bifurcation point BP.

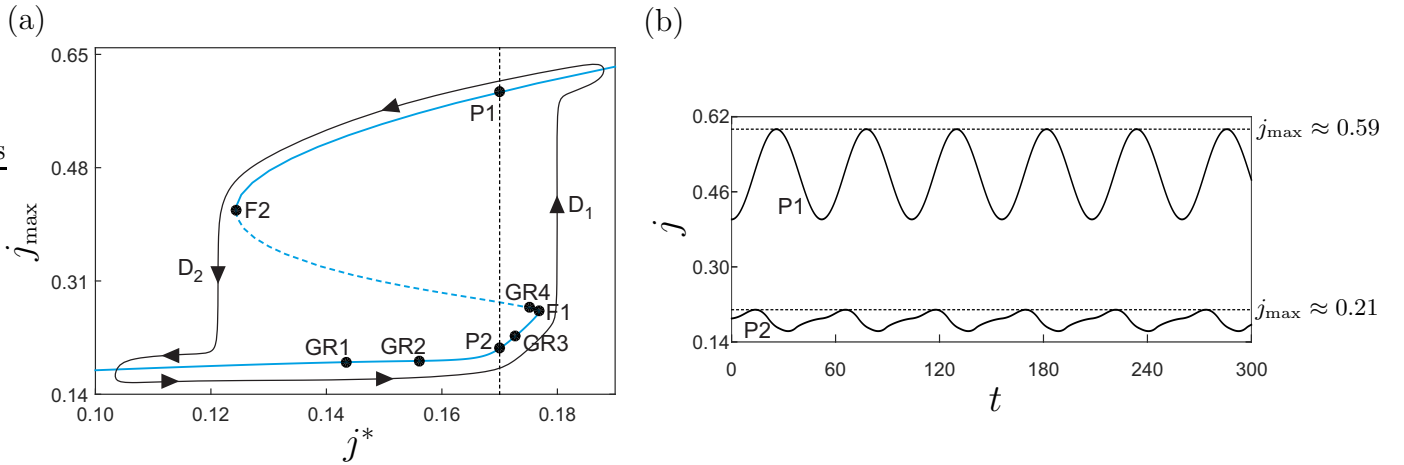


Figure 4: (a) One-parameter continuation of the periodic response shown in Fig. 2(a) with respect to j^* (see (20)). Labels and figure codes are defined as in Fig. 3. (b) Time plot of two (coexisting) stable periodic solutions computed for $j^* = 0.17$ (P_1 , P_2).

Another remarkable feature of the bifurcation diagram shown in Fig. 3(a) is the interplay between the fold bifurcations F1 and F2 giving rise to *hysteresis* in the system, which schematically is represented by the closed curve D₁–D₂ plotted in the figure. Moreover, the fold points F1 and F2 define a parameter window for which the system presents coexisting solutions (see Fig. 3(c)), including the (unstable) disease-free equilibrium. A similar scenario can be observed if now j^* is considered as the bifurcation parameter, see Fig. 4(a). As before, a series of codimension-1 bifurcations are found along the bifurcation diagram, located at $j^* \approx 0.1434$ (GR1, grazing contact with $j = j^*$ from above), $j^* \approx 0.1561$ (GR2, grazing contact with $j = c$), $j^* \approx 0.1727$ (GR3, grazing contact with $j = j^*$ from above), $j^* \approx 0.1751$ (GR4, grazing contact with $j = c$), $j^* \approx 0.1769$ (F1, fold bifurcation) and $j^* \approx 0.1243$ (F2, fold bifurcation). As in the previous case, the interaction between the fold points produces a hysteresis loop, which in turn gives rise to the phenomenon of *multistability*, found for j^* between F2 and F1. For instance, at the initial value $j^* = 0.17$, two stable (endemic) periodic solutions can be found (at the test points P1 and P2), depicted in Fig. 4(b). In the current scenario, the solution at P2 can be identified as a “desirable” solution, owing to the low peak of incidence level ($j_{\max} \approx 0.21$). However, due to the multistability, a sufficiently large perturbation to the system may produce an undesired jump to the solution at P1, for which the peak of incidence level is about three times larger ($j_{\max} \approx 0.59$), hence posing the risk of a collapse of the available medical capabilities. In order to avoid such an undesired scenario, one needs then to set j^* as low as possible (more precisely, below than $j^* \approx 0.1243$ where the fold bifurcation F2 occurs), which defines the point where the media gives regular reports among the susceptible subpopulation thereby encouraging people to take preventive measures.

The last part of the numerical study consists of investigating the behavior of the model as the adiabatic parameter ϵ varies. The result is presented in Fig. 5 using parameter values in Tab. 1. When the seasonal forcing is deactivated, Section 3.2 has shown how nearby solution trajectories approach the locally attractive slow manifold ($\epsilon > 0$) before approaching the critical manifold and ultimately stable equilibria, due to the slaving condition. Panels (a) and (b) depict the preceding phenomenon for different realizations of ϵ . The first-order (red curve) and second-order approximation of the slow manifold (blue curve) are presented in the figure, whereby the two approximates and the actual slow manifold meet and are close to the critical manifold as ϵ is sufficiently small (Panel (b)). Panel (a) exclusively shows how the higher-order terms surpass the influence of ϵ in the approximates, making them irregularly jumping around as ϵ is rather large. This irregularity is worsened by the fact that the model involves a piecewise-smooth vector field. Panels (c) and (d) are obtained via one-parameter continuation of the periodic solution P1 displayed in Fig. 3(c), using ϵ as the control parameter. The numerical study reveals that the (peak-to-peak) amplitude of the periodic solutions does not vary significantly for ϵ small. This behavior, however, notably changes when ϵ crosses a certain threshold $\epsilon_c \approx 0.0021$, when $\zeta = 7560$. From this point on, the amplitude decreases proportionally to $1/\epsilon^2$, as can be seen in Fig. 5(c). This critical value can be computed from (3) as (neglecting transients and considering that $\theta = \mu/\epsilon$ and $\rho = \rho_\epsilon/\epsilon$), which is given by

$$\epsilon_c = 10 \frac{\mu \zeta}{\xi}.$$

This gives the ϵ -value for which the constant component (\bar{M}) becomes ten times the amplitude of seasonality (ζ). This means that for $\epsilon \geq \epsilon_c$, the seasonal effects become less significant, and therefore the amplitude of the periodic solutions decreases with ϵ . The quadratic decrement can be seen from (4), (5) and (6), hence producing a periodic excitation with amplitude proportional to $1/\epsilon^2$. The preceding finding provides additional novelty as apposed to the result in Section 3.4 where $\epsilon \geq \mu \zeta / \xi \sqrt{\theta^2 + 4\pi^2 \omega^2} \approx 3.6 \mu \zeta / \xi > \epsilon_c / 10$ makes the second-order approximations eligible for replacing the actual periodic solutions.

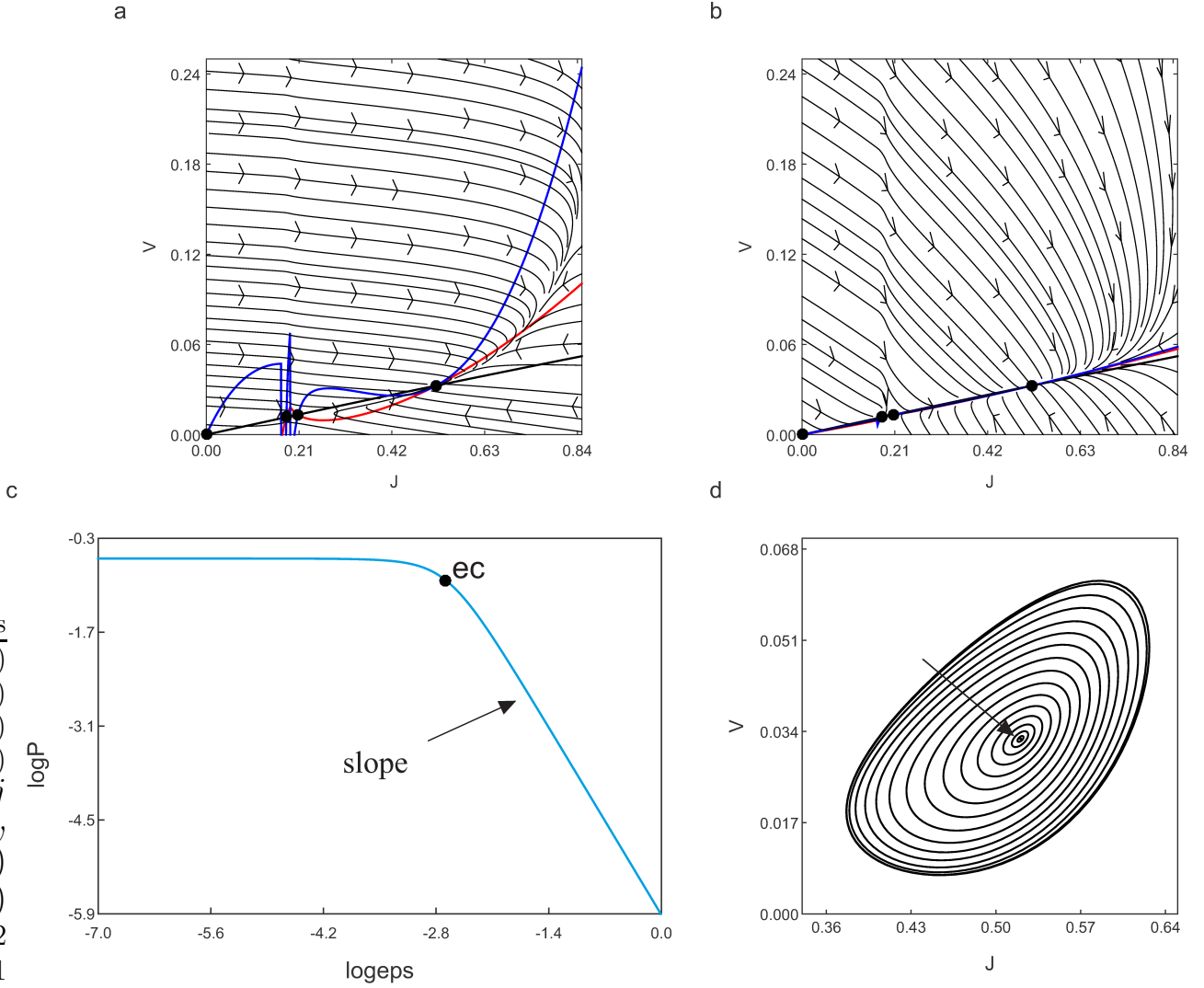


Figure 5: Behavior of the model as the adiabatic parameter (vector–host lifespan ratio) ϵ varies. Panels (a) and (b) show phase portraits around the first-order (red curve), second-order approximation of the slow manifold (blue curve) and the critical manifold (black curve) computed for $\epsilon = 10^{-2}$ and $\epsilon = 10^{-3}$, respectively. The small black circles encode the existing equilibria, where the slow and critical manifold intersect. Panel (c) shows the behavior of the peak-to-peak amplitude (see (31)) of the periodic solution P1 displayed in Fig. 3(c). Panel (d) depicts the family of periodic solutions obtained along the curve in (c). The arrow indicates the direction of increasing ϵ .

7 Conclusion

In a rundown, the following work is done in the paper. We reduce and rescale the simple host–vector, SISUV model into an IU model. A periodic recruitment rate of the vector population is assigned to take into account the influence of meteorological factors. The argument about infected hosts kept in hospitals tells us that the infection rate due to a contact between a susceptible vector and an infected host is constant and sufficiently small. The other infection rate from a typical contact between a susceptible host and an infected vector is modelled as a function of the infected host subpopulation. Under further assumptions, we designate a singular perturbed system under the variation of the vector–host lifespan ratio. In further examination, we center our work around understanding the interplay between the media-triggered infection rate, the periodic solutions surrounding equilibria of the autonomous system, and the lifespan ratio variation. Two scenarios for the infection rate are considered in this regard. The first scenario puts forward a non-increasing infection rate, where the entire stability analysis returns a supercritical bifurcation. Moreover, a larger alarming incidence level j^* has been shown to give a larger endemic equilibrium at the same magnitude of the basic reproductive

number. Keeping in mind the existence of the two notable equilibria, two periodic solutions exist surrounding the equilibria, i.e. when the seasonal forcing is activated. The second scenario presents a new definition for the alarming incidence level j^* , i.e. a maximal number of infected population share the available hospitals can accommodate. This builds up an outline where the infection rate decreases when $j > j^*$, but not long after at $c > j^*$, poverty, reluctance in taking up preventive measures, despair, tiresomeness, perceiving the disease as being easily curable, absence of medical access, and the exploding number of hungrier vectors make the infection rate start to bounce up and gets larger with the incidence level.

The following results are underlying regarding the second scenario. We found a supercritical bifurcation when the basic reproductive number is equal to one, also two fold bifurcations corresponding to the switch from stable to unstable also from unstable to stable endemic equilibrium branch. A similar result is also found from numerical investigation over the stability of the existing periodic solutions. For both autonomous and non-autonomous case, we acquire a hysteresis loop. When the initial infection rate β_0 (or eventually the basic reproductive number) increases, the presence of *overreaction* among the susceptible subpopulation attributed to media reports helps suppress the endemicity level to a small order of magnitude. Until then, β_0 is large enough that the endemicity level jumps to a significantly larger value. We found that the closer c and j^* are, the higher the possibility of encountering such a hysteresis. In contrast, when c is in the far right of j^* , only a small endemic equilibrium can be obtained. All these mean that overreaction is a bad response to the ever-increasing outbreak, as a slow pace with sureness in the longevity and regularity in applying preventive measures can have a better solution. A similar investigation over j^* also gives a hysteresis, therefore a sudden jump to a larger value in the endemicity level. Notwithstanding the new definition for the alarming incidence level, which the decision maker can always make up, we come to the same conclusion as in the first model for the infection rate. We have shown that overestimating alarming incidence level provides a good solution to reduce the endemicity rather underestimating it, in any way. When j^* is sufficiently small, we have shown that no jump to a blow-up is envisaged, also that the endemicity can be suppressed as low as possible. As far as the lifespan ratio ϵ is concerned, it turns to give us flexibility in designing the model as to have solutions that may be comparable to empirical data. For the sample case $\mu\zeta/\xi\sqrt{\theta^2 + 4\pi^2\omega^2} \approx 3.6\mu\zeta/\xi \approx 7.56 \times 10^{-4} < \epsilon = 10^{-3} < \epsilon_c \approx 2.1 \times 10^{-3}$, we know that the critical manifold gives a quite good approximation to the solution, whereby a second-order approximation for the periodic solutions can be chosen for fast computation on an extremely large time domain. We acquire both model reduction and small-order approximation at the same time. Data assimilation using this model with periodic datasets can be possible outlook.

Declaration of Competing Interest

No conflict of interest exists in the submission of this manuscript.

Acknowledgements

The second author has been supported by the DAAD Visiting Professorships programme at the University of Koblenz-Landau. The third author is supported by the Ministry of Research, Technology and Higher Education of the Republic of Indonesia (Kemenristek DIKTI) with PUPIT research grant scheme.

References

- [1] D. J. Gubler, *Insects in Disease Transmission*. Hunter Tropical Medicine, Philadelphia: W B Saunders Co, 7 ed., 1991.
- [2] D. J. Gubler, "Resurgent vector-borne diseases as a global health problem," *Emerging Infectious Diseases*, vol. 4, no. 3, pp. 442–450, 1998.

- [3] D. J. Gubler, “Vector-borne diseases,” *Revue Scientifique et Technique*, vol. 28, no. 2, pp. 583–588, 2009.
- [4] V. Sluydts, L. Durnez, S. Heng, C. Gryseels, L. Canier, S. Kim, K. V. Roey, K. Kerkhof, N. Khim, S. Mao, S. Uk, S. Sovannaroth, K. P. Grietens, T. Sochantha, D. Menard, and M. Coosemans, “Efficacy of topical mosquito repellent (picaridin) plus long-lasting insecticidal nets versus long-lasting insecticidal nets alone for control of malaria: a cluster randomised controlled trial,” *The Lancet Infectious Diseases*, vol. 16, no. 10, pp. 1169–1177, 2016.
- [5] L. Kamareddine, “The Biological Control of the Malaria Vector,” *Toxins*, vol. 4, no. 9, pp. 748–767, 2012.
- [6] K. P. Wijaya, D. Aldila, and L. E. Schäfer, “Learning the seasonality of disease incidences from empirical data,” *Ecological Complexity*, vol. 38, pp. 83–97, 2019.
- [7] M. Salathé and S. Khandelwal, “Assessing vaccination sentiments with online social media: Implications for infectious disease dynamics and control,” *PLoS Computational Biology*, vol. 7, no. 10, pp. e1002199(1)–10, 2012.
- [8] W. Zhou, Y. Xiao, and J. M. Heffernan, “Optimal media reporting intensity on mitigating spread of an emerging infectious disease,” *PLoS ONE*, vol. 14, no. 3, pp. e0213898–18, 2019.
- [9] S. Collinson and J. M. Heffernan, “Modelling the effects of media during an influenza epidemic,” *BMC Public Health*, vol. 14, no. 1, pp. 376–10, 2014.
- [10] S. Collinson, K. Khan, and J. M. Heffernan, “The effects of media reports on disease spread and important public health measurements,” *PLoS ONE*, vol. 10, no. 11, pp. e0141423–21, 2015.
- [11] B.-K. Yoo, M. L. Holland, J. Bhattacharya, C. E. Phelps, and P. G. Szilagyi, “Effects of mass media coverage on timing and annual receipt of influenza vaccination among medicare elderly,” *Health Research and Educational Trust*, vol. 45, no. 5, pp. 1287–1309, 2010.
- [12] M. S. Rahman and M. L. Rahman, “Media and education play a tremendous role in mounting aids awareness among married couples in bangladesh,” *AIDS Research and Therapy*, vol. 4, pp. 10–7, 2007.
- [13] F. H. Chen, “Modeling the effect of information quality on risk behavior change and the transmission of infectious diseases,” *Mathematical Biosciences*, vol. 217, pp. 125–133, 2009.
- [14] A. Sharma and A. K. Misra, “Modeling the impact of awareness created by media campaigns on vaccination coverage in a variable population,” *Journal of Biological Systems*, vol. 22, no. 2, pp. 249–270, 2014.
- [15] Y. Liu and J.-A. Cui, “The impact of media coverage on the dynamics of infectious disease,” *International Journal of Biomathematics*, vol. 1, no. 1, pp. 65–74, 2008.
- [16] Y. Li and J. Cui, “The effect of constant and pulse vaccination on sis epidemic models incorporating media coverage,” *Communications in Nonlinear Science and Numerical Simulation*, vol. 14, no. 5, pp. 2353–2365, 2009.
- [17] Y. Zhao, L. Zhang, and S. Yuan, “The effect of media coverage on threshold dynamics for a stochastic SIS epidemic model,” *Physics A*, vol. 512, pp. 248–260, 2018.
- [18] J. Cui, Y. Sun, and H. Zhu, “The impact of media on the control of infectious diseases,” *Journal of Dynamics and Differential Equations*, vol. 20, no. 1, pp. 31–53, 2007.
- [19] R. Liu, J. Wu, and H. Zhu, “Media/psychological impact on multiple outbreaks of emerging infectious diseases,” *Computational and Mathematical Methods in Medicine*, vol. 8, no. 3, pp. 153–164, 2007.

- [20] J.-A. Cui, X. Tao, and H. Zhu, “An SIS infection model incorporating media coverage,” *Rocky Mountain Journal of Mathematics*, vol. 38, no. 5, pp. 1323–1334, 2008.
- [21] G. O. Agaba, Y. N. Kyrychko, and K. B. Blyuss, “Dynamics of vaccination in a time-delayed epidemic model with awareness,” *Mathematical Biosciences*, vol. 294, pp. 92–99, 2017.
- [22] F. A. Basir, S. Ray, and E. Venturino, “Role of media coverage and delay in controlling infectious diseases: A mathematical model,” *Applied Mathematics and Computation*, vol. 337, pp. 372–385, 2018.
- [23] A. K. Misra, A. Sharma, and J. B. Shukla, “Modeling and analysis of effects of awareness programs by media on the spread of infectious diseases,” *Mathematical and Computer Modelling*, vol. 53, pp. 1221–1228, 2011.
- [24] A. K. Misra, A. Sharma, and V. Singh, “Effect of awareness program in controlling the prevalence of an epidemic with time delay,” *Journal of Biological Systems*, vol. 19, no. 2, pp. 389–402, 2011.
- [25] D. Greenhalgh, S. Rana, S. Samanta, T. Sardar, S. Bhattacharya, and J. Chattopadhyay, “Awareness programs control infectious disease – multiple delay induced mathematical model,” *Applied Mathematics and Computation*, vol. 251, pp. 539–563, 2015.
- [26] S. M. Babin, “Weather and climate effects on disease background levels,” *Johns Hopkins APL Technical Digest*, vol. 24, no. 4, pp. 343–348, 2003.
- [27] L. M. Bartley, C. A. Donnelly, and G. P. Garnett, “The seasonal pattern of dengue in endemic areas: mathematical models of mechanisms,” *Transactions of the Royal Society of Tropical Medicine and Hygiene*, vol. 96, pp. 387–397, 2002.
- [28] D. J. Bicouta, M. Vautrina, C. Vignollesb, and P. Sabatier, “Modeling the dynamics of mosquito breeding sites vs rainfall in Barkedji area, Senegal,” *Ecological Modelling*, vol. 317, pp. 41–49, 2015.
- [29] Y. L. Cheong, K. Burkart, P. J. Leitao, and T. Lakes, “Assessing weather effects on dengue disease in malaysia,” *Int. J. Environ. Res. Public Health*, vol. 10, no. 12, pp. 6319–6334, 2013.
- [30] P.-C. Wu, H.-R. Guo, S.-C. Lung, C.-Y. Lin, and H.-J. Su, “Weather as an effective predictor for occurrence of dengue fever in taiwan,” *Acta Tropica*, vol. 103, no. 1, pp. 50–57, 2007.
- [31] S. Wongkoon, M. Jaroensutasinee, and K. Jaroensutasinee, “Distribution, seasonal variation and dengue transmission prediction in sisaket, thailand,” *Indian Journal of Medical Research*, vol. 138, no. 3, pp. 347–353, 2013.
- [32] L. Esteva and C. Vargas, “Analysis of a dengue disease transmission model,” *Mathematical Biosciences*, vol. 150, no. 2, pp. 131–151, 1998.
- [33] A. Jain and U. C. Chaturvedi, “Dengue in infants: an overview,” *FEMS Immunology & Medical Microbiology*, vol. 59, no. 2, pp. 119–130, 2010.
- [34] C. Kuehn, *Multiple Time Scale Dynamics*, vol. 191 of *Applied Mathematical Sciences*. Springer International Publishing, 2015.
- [35] H. K. Khalil, *Nonlinear Systems*. Prentice Hall, 3 ed., 2002.
- [36] F. Verhulst, “Singular perturbation methods for slow–fast dynamics,” *Nonlinear Dynamics*, vol. 50, no. 4, pp. 747–753, 2007.
- [37] N. Fenichel, “Geometric singular perturbation theory for ordinary differential equations,” *Journal of Differential Equations*, vol. 31, no. 1, pp. 53–98, 1979.

- [38] C. K. R. T. Jones, “Geometric singular perturbation theory,” in *Dynamical Systems* (R. Johnson, ed.), vol. 1609 of *Lecture Notes in Mathematics*, pp. 44–118, Springer Berlin–Heidelberg, 2006.
- [39] H. G. Kaper and T. J. Kaper, “Asymptotic analysis of two reduction methods for systems of chemical reactions,” *Physica D*, vol. 165, pp. 66–93, 2002.
- [40] T. C. Sideris, *Ordinary Differential Equations and Dynamical Systems*. Atlantis Studies in Differential Equations, Atlantis Press, 2013.
- [41] P. Srichan, S. L. Niyom, O. Pacheun, S. Lamsirithawon, S. Chatchen, C. Jones, L. J. White, and W. Pan-ngum, “Addressing challenges faced by insecticide spraying for the control of dengue fever in bangkok, thailand: a qualitative approach,” *International Health*, vol. 10, no. 5, pp. 349–355, 2018.
- [42] L. P. Wong and S. A. Bakar, “Health beliefs and practices related to dengue fever: A focus group study,” *PLoS Neglected Tropical Diseases*, vol. 7, no. 7, pp. e2310–9, 2013.
- [43] S. Sim, J. L. Ramirez, and G. Dimopoulos, “Dengue virus infection of the aedes aegypti salivary gland and chemosensory apparatus induces genes that modulate infection and blood-feeding behavior,” *PLoS Pathogens*, vol. 8, no. 3, pp. e1002631–15, 2012.
- [44] M. di Bernardo, C. J. Budd, A. R. Champneys, and P. Kowalczyk, *Piecewise-smooth dynamical systems. Theory and Applications*, vol. 163 of *Applied Mathematical Sciences*. New York: Springer-Verlag, 2004.
- [45] P. Thota and H. Dankowicz, “TC-HAT: A novel toolbox for the continuation of periodic trajectories in hybrid dynamical systems,” *SIAM Journal of Applied Dynamical Systems*, vol. 7, no. 4, pp. 1283–1322, 2008.
- [46] H. Dankowicz and F. Schilder, *Recipes for Continuation*. Computational Science and Engineering, Philadelphia: SIAM, 2013.
- [47] B. Krauskopf, H. M. Osinga, and J. Galán-Vioque, eds., *Numerical Continuation Methods for Dynamical Systems*. Understanding Complex Systems, Netherlands: Springer-Verlag, 2007.